Trapped Alkali-Metal Rydberg Qubit

Y. Mei, Y. Li, H. Nguyen, P. R. Berman, and A. Kuzmich*
Department of Physics, University of Michigan, Ann Arbor, Michigan 48109, USA

(Received 10 November 2021; accepted 17 February 2022; published 22 March 2022)

Rydberg interactions of trapped alkali-metal atoms are used widely to facilitate quantum gate operations in quantum processors and repeaters. In most laboratory realizations using this protocol, the Rydberg states are repelled by the trapping laser fields, requiring that the fields be turned off during gate operations. Here we create a quasi-two-level system in a regime of Rydberg excitation blockade for a mesoscopic Rb ensemble of several hundred atoms confined in a magic-wavelength optical lattice. We observe many-body Rabi oscillations between the ground and collective Rydberg state. In addition we use Ramsey interference techniques to obtain the light shifts of both the lower and upper states of the collective qubit. Whereas the coupling producing the Rabi oscillations is enhanced by a factor of $\sqrt{N}$, there is no corresponding enhancement for the light shifts. We derive an effective two-level model which is in good agreement with our observations. Trapped Rydberg qubits and an effective two-level description are expected to have broad applicability for studies of quantum simulation and networking using collective encoding in ensembles of neutral atoms.

DOI: 10.1103/PhysRevLett.128.123601

Quantum technologies offer transformative advances in storage, processing, and communication of information compared to established classical approaches. The recipe for combining distant quantum processors into a single quantum network involves three key ingredients: qubits, quantum logic for entanglement generation and correction, and interaction interfaces [1,2]. Neutral atomic ensembles are a strong candidate to serve as a basis for scalable quantum networks [3–6]. Collective qubits based on atomic hyperfine ground states can be converted, on demand, into single photons [7], making them well-suited for scalable quantum network-type protocols over telecom-wavelength optical fibers [8,9]. Notably, collective atomic qubit states between ground and Rydberg states can be deterministically created and coherently manipulated in the regime of the excitation blockade [10–18], allowing for dramatically faster remote entanglement generation compared with probabilistic approaches [19,20].

In order to use the Rydberg blockade in quantum information processing, the (optical) ground-Rydberg atomic coherence must be preserved. Ideally, this is achieved if the atoms are confined in a potential $U(\mathbf{r})$ that is identical for the ground and the Rydberg levels. However, in a regular far-off-resonance optical dipole trap, e.g., based on a 1064 nm laser for Rubidium atoms, the spatially inhomogeneous energy shifts $U(\mathbf{r})$ are entirely different for the ground and Rydberg states. For (trapped) ground-level atoms, the dynamic polarizability in a (red-detuned) light field is positive, whereas Rydberg electrons are nearly free, and their polarizability is approximately equal to that of a free electron, which is negative. This means that atoms in Rydberg states are antitrapped since they are pushed out of the laser field intensity maxima. This problem leads to the necessity of shutting off the trap fields for the duration of quantum operations. The repeated process of turning the trap fields on and off heats the atoms and dramatically shortens their lifetime to μs, limiting its utility [21,22].

In a state-insensitive (or "magic-wavelength") trap proposal of Refs. [23,24], the frequency of an optical lattice is tuned to the blue side of an atomic resonance from the Rydberg level to an intermediate level, creating positive polarizability of the Rydberg level. For example, if the (1012 nm) lattice field is detuned by $\simeq(52/n)^3$ GHz from the $|nS_{1/2}\rangle \leftrightarrow |6P_{3/2}\rangle$ transition in atomic Rb, the depth of the trapping potentials for the ground- and Rydberg-level atoms are approximately equal. This method has been demonstrated by our group [25–27] and by Goldschmidt *et al.* [28]. More recently, trapped single-atom Rydberg qubits have been demonstrated in alkaline-earth atoms [29].

Here we report observations of dynamics of a Rydberg qubit encoded in an ensemble of $\sim 10^3$ atoms that are confined in a state-insensitive optical lattice trap. We observe coherent driving and Ramsey interference measurements of light shifts induced on either the lower or the upper qubit state, on timescales of order ~ 10 μs. The dynamics of the trapped qubit and the light shifts are well described by an effective two-level model with possible dephasing factors included, i.e., laser phase noise, atom number fluctuation, and so on. The experimental setup is shown in Fig. 1(a). ^{87}Rb atoms are collected in a magneto-optical trap (MOT) and are subsequently loaded into a far-off resonance (YAG, 1064 nm) cross-dipole trap. The longitudinal extent of the atomic cloud is ~ 10 μm along

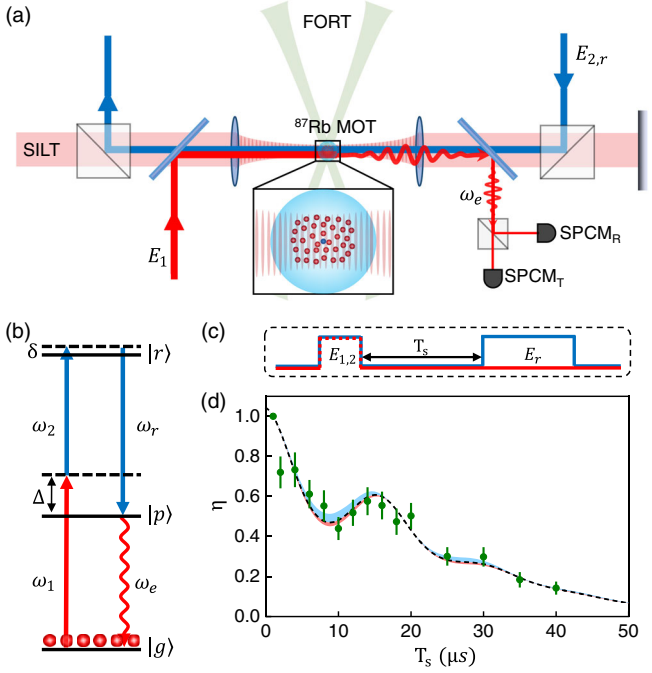

FIG. 1. (a) Experimental setup: an ultracold ^{87}Rb atomic ensemble is prepared in a one-dimensional state-insensitive lattice trap (SILT) formed by a 1012 nm retroreflected beam using atoms that have been transferred from a crossed far-off-resonance dipole trap (FORT) formed by focused yttrium aluminum-garnet (YAG) laser beams. Excitation fields E_1 (780 nm) and E_2 (480 nm) drive atoms from $|g\rangle$ to $|p\rangle$ and from $|p\rangle$ to $|r\rangle$, respectively. A retrieval pulse E_r leads to phase-matched emission that is coupled into a pair of single-mode fibers and subsequently measured by single-photon counting modules SPCM$_T$ and SPCM$_R$. (b) Single atom energy levels for ^{87}Rb: $|g\rangle = |5S_{1/2}, F = 2, m_F = -2\rangle$, $|p\rangle = |5P_{3/2}, F = 3, m_F = -3\rangle$, and $|r\rangle = |nS_{1/2}, m_J = -1/2\rangle$. (c) Timing sequence for the ground-Rydberg spin-wave coherence measurement. (d) Normalized signal η as a function of storage time T_s for quantum number $n = 75$. The storage efficiency is normalized to that at 1 μs. Blue and red bands represent temperatures 40% lower and higher than the best-fit value, respectively.

the excitation field direction. Next, the atoms are transferred from the crossed dipole trap to a state-insensitive optical lattice. The lattice is formed by a horizontally polarized and retroreflected laser field, which is detuned from the $|6P_{3/2}\rangle \leftrightarrow |75S_{1/2}\rangle$ transition by $\Delta_m/2\pi \simeq 367$ MHz—the so-called "magic" value of the detuning for which the potential depths for the ground and the Rydberg atomic states are equal. After the transfer, the lattice depth is adiabatically lowered.

The atoms are driven by laser fields E_1 (780 nm, σ^-) and E_2 (480 nm, σ^+) from the ground state $|g\rangle = |5S_{1/2}, F = 2, m_F = -2\rangle$ to the Rydberg state $|r\rangle = |75S_{1/2}, m_J = -1/2\rangle$ with a detuning of $\Delta/2\pi = 480$ MHz from the intermediate state $|p\rangle = |5P_{3/2}, F = 3, m_F = -3\rangle$, with respective Rabi frequencies Ω_1 and Ω_2, Fig. 1(b). In the Rydberg excitation blockade regime, ideally, the atoms will undergo an oscillation between two collective (Dicke) atomic states, $|0\rangle = \prod_{i=1}^{N} |g_i\rangle$ and $|1\rangle = (1/\sqrt{N}) \sum_{i=1}^{N} e^{i(\mathbf{k_1}+\mathbf{k_2})\cdot\mathbf{r_i} - i(\omega_1+\omega_2)t} |g_1 \ldots r_i \ldots g_N\rangle$, where N is the total number of atoms participating in the many-body blockade. After a controllable delay, T_s, following the excitation pulse, a readout pulse E_r (with Rabi frequency Ω_r) that is resonant with the $|r\rangle$ to $|p\rangle$ transition frequency is applied and leads to phase-matched emission having frequency ω_e (see the Supplemental Material [30] for experimental details).

We model our system as an effective two-level system with a closed transition between the states $|0\rangle$ and $|1\rangle$ [30]. The collective Rabi frequency of this two-state model is $\Omega_N = \sqrt{N}\Omega$, where $\Omega = (\Omega_1\Omega_2/2\Delta)$ is the effective two-photon, single-atom Rabi frequency. With the two-photon detuning δ set equal to zero, the population of the many-body Rydberg state $|1\rangle$ is $\rho_{11} = \frac{1}{2}(1 - e^{-\frac{\gamma_1}{2}T_p} \cos\sqrt{N}\Omega T_p)$, where T_p is the pulse duration of a constant amplitude pulse whose pulse area is equal to that of the actual pulse. We have incorporated dephasing from relaxation processes such as that produced by laser frequency noise into our model by assuming that the coherence ρ_{01} decays at rate γ_1, which agrees well with the measured laser linewidth in our system [30]. The intensity of the retrieved signal is proportional to this population.

To describe the combined effects of spin-wave dephasing and loss of the Rydberg state component, we include an overall exponential damping of the retrieved signal $\sim e^{-\alpha(T_s+T_p)}$. We account for fluctuations in atomic number by weighting the retrieved signal with the probability distribution $f(k, N)$ to have k atoms in the interaction volume when the average number in the volume is N. On averaging over k for the Poisson distribution $f(k) = (N^k e^{-N}/k!)$, we find that the oscillation amplitude is damped by a factor $\exp(-T_P^2/\tau_1^2)$, where $\tau_1 = 2\sqrt{2}/\Omega$, and that the photoelectric detection probability per trial p_1 for the retrieved signal is given by

$$p_1 \simeq \frac{1}{2}\xi e^{(-\alpha(T_p+T_S))}(1 - e^{-\frac{\gamma_1}{2}T_p} e^{-T_p^2/\tau_1^2} \cos\sqrt{N}\Omega T_p), \quad (1)$$

where ξ is the overall retrieval and detection efficiency. Intensity fluctuations of the driving fields would also damp the oscillation visibility, but these effects are negligible in our experiment (see Ref. [30] for details for the intensity stabilization).

The normalized storage efficiency η [26,30] is plotted as a function of storage period T_s for $T_p = 1\,\mu s$ and a trap depth of $\simeq 40$ μK in Fig. 1(c), showing that the coherence lifetime for the ground-Rydberg coherence can be extended up to $\simeq 20$ μs, which is an order of magnitude improvement over that achieved with atomic ensembles in free space [the oscillation in the figure is due to motional effects not included in Eq. (1)] [11–13,22,25]. The longer lifetime

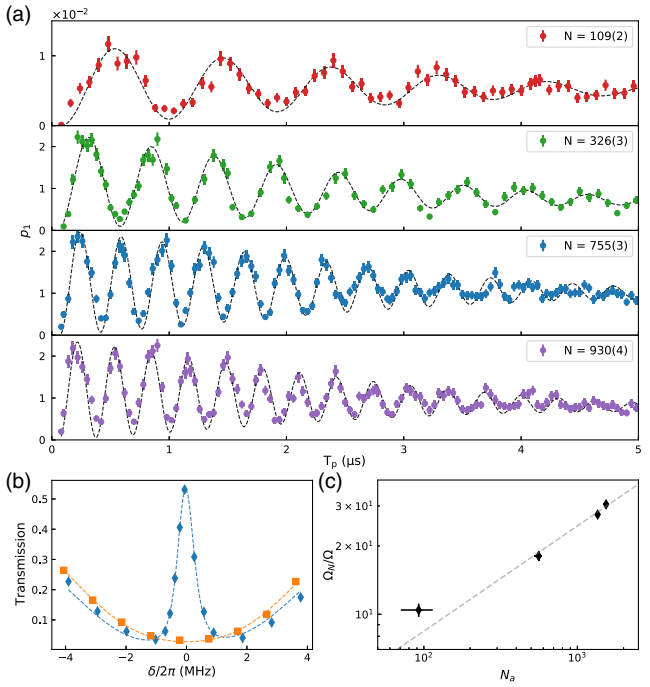

FIG. 2. (a) Collective Rabi oscillation as a function of the pulse duration T_p for different numbers of atoms. Red: $N = 109(2)$; green: $N = 326(3)$; blue: $N = 755(3)$; purple: $N = 930(4)$. Here, $\Omega_1/2\pi = 9.2$ MHz, $\Omega_2/2\pi = 10.8$ MHz, and $\Omega_r/2\pi = 11.5$ MHz. The dashed lines are theoretical results using an effective two-state model. The error bars represent one standard deviation ($\sqrt{M}$) for M photoelectric counting events. (b) Probe transmission (orange squares) and EIT (blue diamonds) measurement for $N = 755(9)$, consistent with an OD = 3.5. (c) The enhancement of the collective Rabi frequency Ω_N/Ω as a function of number of atoms N_a determined by the absorption measurement. The data are fit with a function $\Omega_N = \Omega N_a^k$ with the best-fit value $k = 0.463(5)$. The error bars represent the standard errors of the respective fits.

allows us to vary the excitation pulse duration to tens of μs, instead of varying the excitation field strength as we did previously [12]. As a result, the light shifts caused by the excitation laser fields can be kept constant over the extent of the measurement. The methods we employ to control laser phase noise and intensity fluctuations, to reduce electric field shifts, to minimize atom number variation or loss, and to suppress the effects of atomic thermal motion are outlined in Ref. [30].

The population of the upper qubit state is measured by mapping it into a phase-matched retrieved field. To measure the dependence of the collective Rabi frequency on density, the associated photoelectric detection probabilities per trial p_1 are recorded as a function of the excitation pulse duration time T_p, while the storage period $T_s = 1$ μs is kept constant. In Fig. 2, the resulting collective Rabi oscillations are shown for a lattice trap depth of 60 μK for varying atomic density, controlled by altering the YAG power. As expected, the oscillation frequency increases with the atomic density, but all the signals vanish within 5 μs, due to the limitation of $\tau_1 \approx 4.3$ μs. The dashed curves are theory fits based on Eq. (1). As the YAG power is raised up from 6 W to 35 W, the fitted value for the number of atoms N increases from $\simeq 10^2$ to $\simeq 10^3$. The fit value for the global dephasing factor $\gamma_1/2\pi \simeq 40$ kHz is consistent with the laser linewidth estimated from the excitation spectra [30]. The best fit for α for all four sets of data is $\alpha/2\pi \approx 0.008$ MHz, which agrees with the coherence time of 20 μs shown in Fig. 1(c).

For an independent determination of the atom number and single-atom Rabi frequency, we measure the atomic density using absorption of a transmitted probe field, both with and without a control-EIT (electromagnetic-induced transparency) field. For example, the measured optical depth (OD) of $\simeq 3.5$ for a YAG power of 20 W that can be extracted from the transmission curves shown in Fig. 2(b) corresponds to an atomic density having peak value of 2.9×10^{11} cm^{-3}. In Fig. 2(c) we plot the normalized collective Rabi frequency Ω_N/Ω as a function of the number of atoms N_a in the interaction volume (see Ref. [30] for details). We confirm the collective Rabi frequency Ω_N is enhanced by a factor $\sqrt{N}$ with respect to the single-atom value, by fitting the function $\Omega_N = \Omega N_a^k$ and finding a best-fit value $k = 0.463(5)$. The discrepancy for low atom numbers results from a relatively large error of OD fit value when the absorption is small.

We confirm that the Rydberg blockade is fully operational in our system by measuring the second-order autocorrelation function $g^{(2)}(0) < 0.2$ within the time interval of Rabi oscillations [Fig. 3] and demonstrate the multiparticle entanglement [41–43] of the W state $|1\rangle$ within the ensemble [30]. To investigate the main contributions to the damping of the Rabi oscillations, we vary the Rabi frequency and the atom number in a shallower trap depth of 40 μK to minimize the effects of atomic thermal motion and collisions. In Fig. 3(a), obtained with a lower Rabi frequency, 9 oscillations occur within a time window of 12 μs. Approximately four times higher Rabi frequency, but fewer atoms in the blockade volume are used for data in Fig. 3(b). In this limit, 13 oscillation cycles are damped within $\simeq 6$ μs. These results indicate that in the case of Fig. 3(a), the dephasing is due mainly to the dephasing parameter γ_1 term. If this parameter is set equal to zero [resulting in the dotted line in Fig. 3(a)], the oscillations damp more slowly than the data, while the atom number fluctuations have little impact on the visibility damping [resulting in the dash-dotted line in Fig. 3(a)]. In the case of Fig. 3(b), the damping of the oscillations can be ascribed chiefly to the Poisson distribution of number of atoms, N_e, that limits the visible number of the oscillation periods. If atom number fluctuations are neglected [resulting in the dash-dotted line in Fig. 3(b)], the oscillations persist for a time longer than the experimental observation period. However, the theory with $\gamma_1 = 0$ [resulting in the dotted

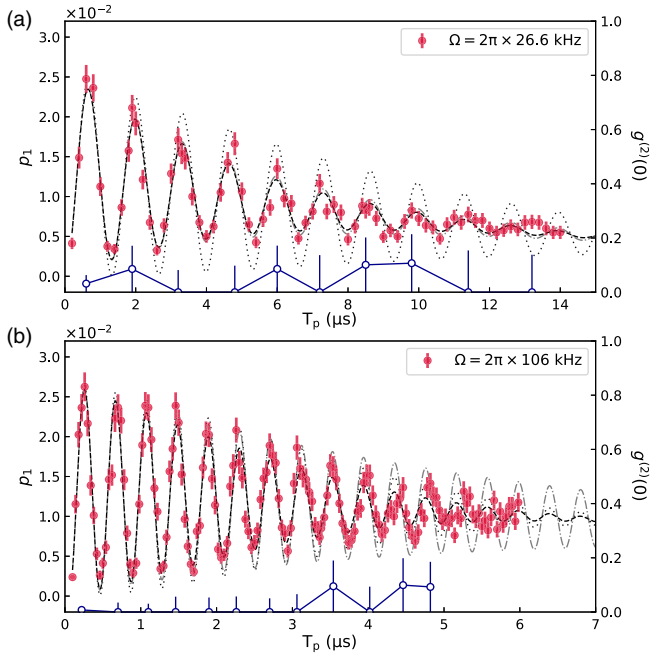

FIG. 3. Collective Rabi oscillation as a function of the pulse duration for different Rabi frequency, (a) $\Omega_1/2\pi = 4.7$ MHz, $\Omega_2/2\pi = 5.4$ MHz, and $N = 797(7)$. (b) $\Omega_1/2\pi = 9.2$ MHz, $\Omega_2/2\pi = 10.8$ MHz, and $N = 553(2)$. The dashed line shows best fit from theory with dephasing and atom number fluctuations. The dotted line shows the simulation without dephasing, and the dash-dotted line shows the simulation without atom number fluctuations. The blue hollow circles represent the second-order intensity correlation function at zero delay $g^{(2)}(0)$, which is below 0.2 within the Rabi oscillations, suggesting a well-established Rydberg blockade.

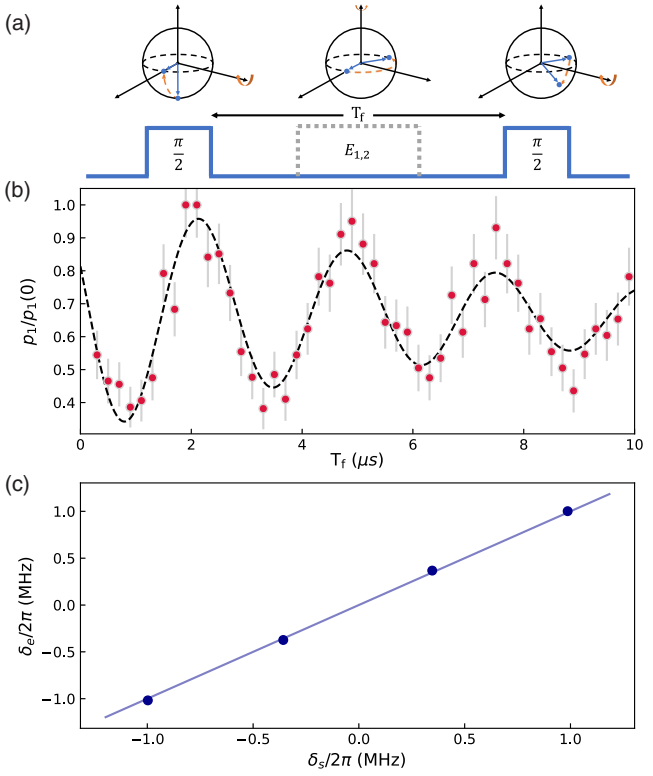

FIG. 4. Ramsey interferometry of the trapped qubit. (a) Schematic and timing sequence. (b) Evolution of the $|1\rangle$ state versus free evolution time T_f between the two $\pi/2$ pulses of detuning $\delta_s/2\pi = -0.3$ MHz and pulse width 0.45 μs. Dashed line represents the sinusoidal fit with an exponential decay. The error bars represent one standard deviation ($\sqrt{M}$) for M photoelectric counting events. (c) The detuning extracted from the sinusoidal fit versus detuning set to ω_1. The line represents the fitted result of $\delta_e = k\delta_s + b$ with $k = 1.022(6)$ and $b = 0.000(6)$ MHz. The error bar of each point is within the size of the marker.

line in Fig. 3(b)] agrees well with the data. These results indicate that a combination of a narrower (e.g., 1 kHz) laser linewidth and a sub-Poisson atom-number distribution [44,45] may be able to prolong the lifetime of the collective Rabi oscillation to tens of microseconds. Notably, with a large intermediate state detuning and a shallow lattice trap depth, spontaneous decay from the Rydberg level and the influence of blackbody radiation can be neglected in our system.

To further investigate the nature of the collective state, we perform Ramsey interferometry. First, we apply two off-resonance $\pi/2$ pulses separated by a variable free evolution time T_f, followed by a phase-matched retrieval of the $|1\rangle$ state population. Using this protocol, we obtain the oscillation of the retrieved signal as a function of T_f shown in Fig. 4(a). In order to explore different Ramsey scenarios, we change the two photon detuning by varying the detuning δ_s of the ω_1 field. We extract the measured detuning δ_e from the oscillation period in the Ramsey interferometry by the fitting equation $p_1/p_1(0) = \frac{1}{2}[1 + \exp(-\gamma T_f)\cos(\delta_e T_f + \phi)]$. The decay time constant $1/\gamma$ for the Ramsey interferometry in Fig. 4(a) is 6.89 ± 1.3 μs. The phase offset $\phi/2\pi = 0.14$ is due to the finite (0.45 μs) duration of the $\pi/2$ pulses. We fit our results using $\delta_e = k\delta_s + b$, with $k = 1.022(6)$ and $b = 2\pi \times 0.000(6)$ MHz [Fig. 4(b)].

To determine whether or not there are any collective light shifts, we add a dressing field E_1 or E_2 during the T_f period. With the presence of the dressing field, the oscillation frequency of the Ramsey interferometry will be changed from δ_e to $\delta_e + \Delta E/\hbar$, where ΔE is the light shift produced by the two excitation fields. As is shown in Ref. [30], it is expected that $\Delta E = \hbar(\Omega_1^2 - \Omega_2^2)/(4\Delta)$, with no enhancement from collective effects. We measure the dependence of ΔE on $\Omega_{1,2}$ by changing the power of the dressing field and observing the change in frequency of the Ramsey interferometry signal. We observe either an increase or a decrease in oscillation frequency as we increase Ω_1 and Ω_2 respectively, as shown in Figs. 5(a) and 5(b). Figure 5(c) shows the light shift induced by different Ω_1 and Ω_2 as well as theory curves, confirming that there is no *relative* collective light shift between the two levels.

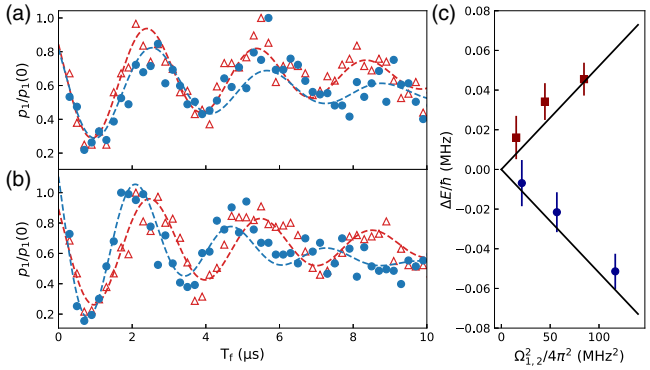

FIG. 5. Ramsey interferometry with dressing field light shift. (a) Ramsey interferometry with (blue circles) and without (red triangles) dressing field of $\Omega_1/2\pi = 3.9$ MHz. (b) Ramsey interferometry with (blue circles) and without (red triangles) dressing field of $\Omega_2/2\pi = 10.8$ MHz. The detuning of the $\pi/2$ pulses is set to $\delta_s/2\pi = -0.3$ MHz. (c) Light shift ΔE versus dressing field Rabi frequency Ω_1 and Ω_2. Red squares represent varying the Ω_1 field and blue circles represent varying the Ω_2 field. Black lines represent the theoretical curve of $\Delta E = \hbar(\Omega_1^2 - \Omega_2^2)/(4\Delta)$.

In summary, we have demonstrated long-lived Rabi oscillations and measured light shifts for a collective Rydberg qubit held in an optical lattice that is state insensitive for the ground and Rydberg levels. Whereas the coupling producing the Rabi oscillations is enhanced by a factor of $\sqrt{N}$, there is no corresponding enhancement for the light shifts. These results provide new evidence that collective Rydberg qubits can be used to create high-fidelity photon-photon gates [10], deterministic single photons [7], and multiple qubits [46] for scalable quantum networking.

The work was supported by the Air Force Office of Scientific Research and the National Science Foundation.

Y. M. and Y. L. contributed equally to this work.

*akuzmich@umich.edu

[1] C. Simon, Towards a global quantum network, Nat. Photonics **11**, 678 (2017).
[2] S. Wehner, D. Elkouss, and R. Hanson, Quantum internet: A vision for the road ahead, Science **362**, eaam9288 (2018).
[3] D. N. Matsukevich and A. Kuzmich, Quantum state transfer between matter and light, Science **306**, 663 (2004).
[4] T. Chanelière, D. N. Matsukevich, S. D. Jenkins, S.-Y. Lan, T. A. B. Kennedy, and A. Kuzmich, Storage and retrieval of single photons transmitted between remote quantum memories, Nature (London) **438**, 833 (2005).
[5] J. K. Thompson, J. Simon, H. Loh, and V. Vuletic, A high-brightness source of narrowband identical-photon pairs, Science **313**, 74 (2006).
[6] Y. A. Chen, S. Chen, Z.-S. Yuan, B. Zhao, C.-S. Chuu, J. Schmiedmayer, and J.-W. Pan, Memory-built-in quantum teleportation with photonic and atomic qubits, Nat. Phys. **4**, 103 (2008).
[7] D. P. Ornelas-Huerta, A. N. Craddock, E. A. Goldschmidt, A. J. Hachtel, Y. Wang, P. Bienias, A. V. Gorshkov, S. L. Rolston, and J. V. Porto, On-demand indistinguishable single photons from an efficient and pure source based on a Rydberg ensemble, Optica **7**, 813 (2020).
[8] A. G. Radnaev, Y. O. Dudin, R. Zhao, H. H. Jen, S. D. Jenkins, A. Kuzmich, and T. A. B. Kennedy, Quantum memory with telecom wavelength conversion, Nat. Phys. **6**, 894 (2010).
[9] Y. O. Dudin, A. G. Radnaev, R. Zhao, J. Z. Blumoff, T. A. B. Kennedy, and A. Kuzmich, Entanglement of Light-Shift Compensated Atomic Spin Waves with Telecom Light, Phys. Rev. Lett. **105**, 260502 (2010).
[10] M. Saffman, T. G. Walker, and K. Mølmer, Quantum information with Rydberg atoms, Rev. Mod. Phys. **82**, 2313 (2010).
[11] Y. O. Dudin and A. Kuzmich, Strongly interacting Rydberg excitations of a cold atomic gas, Science **336**, 887 (2012).
[12] Y. O. Dudin, L. Li, F. Bariani, and A. Kuzmich, Observation of coherent many-body Rabi oscillations, Nat. Phys. **8**, 790 (2012).
[13] M. Ebert, A. Gill, M. Gibbons, X. Zhang, M. Saffman, and T. G. Walker, Atomic Fock State Preparation Using Rydberg Blockade, Phys. Rev. Lett. **112**, 043602 (2014).
[14] L. Li and A. Kuzmich, Quantum memory with strong and controllable Rydberg-level interactions, Nat. Commun. **7**, 13618 (2016).
[15] W. Xu, A. V. Venkatramani, S. H. Cantú, T. Šumarac, V. Klüsener, M. D. Lukin, and V. Vuletić, Fast Preparation and Detection of a Rydberg Qubit Using Atomic Ensembles, Phys. Rev. Lett. **127**, 050501 (2021).
[16] N. L. R. Spong, Y. Jiao, O. D. W. Hughes, K. J. Weatherill, I. Lesanovsky, and C. S. Adams, Collectively Encoded Rydberg Qubit, Phys. Rev. Lett. **127**, 063604 (2021).
[17] H. Levine, A. Keesling, A. Omran, H. Bernien, S. Schwartz, A. S. Zibrov, M. Endres, M. Greiner, V. Vuletic, and M. D. Lukin, High-Fidelity Control and Entanglement of Rydberg-Atom Qubits, Phys. Rev. Lett. **121**, 123603 (2018).
[18] I. S. Madjarov, J. P. Covey, A. L. Shaw, J. Choi, A. Kale, A. Cooper, H. Pichler, V. Schkolnik, J. R. Williams, and M. Endres, High-fidelity entanglement and detection of alkaline-earth Rydberg atoms, Nat. Phys. **16**, 857 (2020).
[19] E. Brion, F. Carlier, V. M. Akulin, and K. Mølmer, Quantum repeater with Rydberg-blocked atomic ensembles in fiber-coupled cavities, Phys. Rev. A **85**, 042324 (2012).
[20] Y. Han, B. He, K. Heshami, C.-Z. Li, and C. Simon, Quantum repeaters based on Rydberg-blockade coupled atomic ensembles, Phys. Rev. A **81**, 052311 (2010).
[21] H. Labuhn, D. Barredo, S. Ravets, S. de Léséleuc, T. Macri, T. Lahaye, and A. Browaeys, Tunable two-dimensional arrays of single Rydberg atoms for realizing quantum Ising models, Nature (London) **534**, 667 (2016).
[22] J. Zeiher, P. Schauß, S. Hild, T. Macrì, I. Bloch, and C. Gross, Microscopic Characterization of Scalable Coherent Rydberg Superatoms, Phys. Rev. X **5**, 031015 (2015).

[23] M. S. Safronova, C. J. Williams, and C. W. Clark, Optimizing the fast Rydberg quantum gate, Phys. Rev. A **67**, 040303 (2003).
[24] M. Saffman and T. G. Walker, Analysis of a quantum logic device based on dipole-dipole interactions of optically trapped Rydberg atoms, Phys. Rev. A **72**, 022347 (2005).
[25] L. Li, Y. O. Dudin, and A. Kuzmich, Entanglement between light and an optical atomic excitation, Nature (London) **498**, 466 (2013).
[26] J. Lampen, H. Nguyen, L. Li, P. R. Berman, and A. Kuzmich, Long-lived coherence between ground and Rydberg levels in a magic-wavelength lattice, Phys. Rev. A **98**, 033411 (2018).
[27] H. Nguyen, J. Lampen, P. R. Berman, and A. Kuzmich, Differential nuclear-spin-dependent light shifts and state mixing of Rydberg atoms, Phys. Rev. A **100**, 033412 (2019).
[28] E. A. Goldschmidt, D. G. Norris, S. B. Koller, R. Wyllie, R. C. Brown, J. V. Porto, U. I. Safronova, and M. S. Safronova, Magic wavelengths for the 5s-18s transition in rubidium, Phys. Rev. A **91**, 032518 (2015).
[29] J. T. Wilson, S. Saskin, Y. Meng, S. Ma, R. Dilip, A. P. Burgers, and J. D. Thompson, Trapping Alkaline Earth Rydberg Atoms Optical Tweezer Arrays, Phys. Rev. Lett. **128**, 033201 (2022).
[30] See Supplemental Material at http://link.aps.org/supplemental/10.1103/PhysRevLett.128.123601 for more theoretical and experimental details, which includes Refs. [31–40].
[31] G. S. Agarwal, Exact Solution for the Influence of Laser Temporal Fluctuations on Resonance Fluorescence, Phys. Rev. Lett. **37**, 1773 (1976).
[32] G. S. Agarwal, Quantum statistical theory of optical-resonance phenomena in fluctuating laser fields, Phys. Rev. A **18**, 1490 (1978).
[33] S. de Lèséleuc, D. Barredo, V. Lienhard, A. Browaeys, and T. Lahaye, Analysis of imperfections in the coherent optical excitation of single atoms to Rydberg states, Phys. Rev. A **97**, 053803 (2018).
[34] P. Cladé, Ph.D. thesis, Université Paris 6, 2004.
[35] X. Jiang, M. Friesen, J. Scott, and M. Saffman, The effect of laser noise on Rabi oscillation fidelity, Bull. Am. Phys. Soc. **66** (2021), https://meetings.aps.org/Meeting/DAMOP21/Session/N01.38.
[36] G. M. Stéphan, T. T. Tam, S. Blin, P. Besnard, and M. Têtu, Laser line shape and spectral density of frequency noise, Phys. Rev. A **71**, 043809 (2005).
[37] Y. Mei, Y. Li, H. Nguyen, P. R. Berman, and A. Kuzmich, Dynamics of interaction-induced dephasing for collective Rydberg excitations (unpublished).
[38] Y. O. Dudin, F. Bariani, and A. Kuzmich, Emergence of Spatial Spin-Wave Correlations in a Cold Atomic Gas, Phys. Rev. Lett. **109**, 133602 (2012).
[39] F. Bariani, Y. O. Dudin, T. A. B. Kennedy, and A. Kuzmich, Dephasing of Multiparticle Rydberg Excitations for Fast Entanglement Generation, Phys. Rev. Lett. **108**, 030501 (2012).
[40] N. Šibalić, J. D. Pritchard, C. S. Adams, and K. J. Weatherill, Arc: An open-source library for calculating properties of alkali Rydberg atoms, Comput. Phys. Commun. **220**, 319 (2017).
[41] F. Fröwis, P. C. Strassmann, A. Tiranov, C. Gut, J. Lavoie, N. Brunner, F. Bussières, M. Afzelius, and N. Gisin, Experimental certification of millions of genuinely entangled atoms in a solid, Nat. Commun. **8**, 907 (2017).
[42] R. McConnell, H. Zhang, J. Hu, S. Cuk, and V. Vuletic, Entanglement with negative Wigner function of almost 3,000 atoms heralded by one photon, Nature (London) **519**, 439 (2015).
[43] F. Haas, J. Volz, R. Gehr, J. Reichel, and J. Estève, Entangled states of more than 40 atoms in an optical fiber cavity, Science **344**, 180 (2014).
[44] Y. Wang, S. Shevate, T. M. Wintermantel, M. Morgado, G. Lochead, and S. Whitlock, Preparation of hundreds of microscopic atomic ensembles in optical tweezer arrays, npj Quantum Inf. **6**, 54 (2020).
[45] S. Whitlock, C. F. Ockeloen, and R. J. C. Spreeuw, Sub-Poissonian Atom-Number Fluctuations by Three-Body Loss in Mesoscopic Ensembles, Phys. Rev. Lett. **104**, 120402 (2010).
[46] M. Khazali and K. Mølmer, Fast Multiqubit Gates by Adiabatic Evolution in Interacting Excited-State Manifolds of Rydberg Atoms and Superconducting Circuits, Phys. Rev. X **10**, 021054 (2020).